EFFECTS of Kr and Xe ION IRRADIATION on the STRUCTURE of Y_2O_3 NANOPRECIPITATES in YBCO THIN FILM CONDUCTORS

Elena I. Suvorova[1*], Oleg V. Uvarov[2], Alexey V. Ovcharov[3], Igor A. Karateev[3], Alexandr L. Vasiliev[1,3], Vladimir A. Skuratov[4,5,6], Philippe A. Buffat[7]

[1] *A.V.Shubnikov Institute of Crystallography, Federal Scientific Research Centre "Crystallography and Photonics" of Russian Academy of Sciences, Leninsky pr., 59, 19333 Moscow, Russia*

[2] *Prokhorov General Physics Institute of Russian Academy of Sciences, Vavilov str., 38, 119991 Moscow, Russia*

[3] *National Research Center "Kurchatov Institute", Akademika Kurchatova pl., 1, 123182 Moscow, Russia*

[4] *FLNR, JINR, 141980 Dubna, Russia*

[5] *National Research Nuclear University MEPhI, Kashirskoe shosse, 31, 115409 Moscow, Russia*

[6] *Dubna State University, Universitetskaja str, 19, 141982 Dubna, Russia*

[7] *Ecole Polytechnique Fédérale de Lausanne, Centre Interdisciplinaire de Microscopie Electronique, Station 12, CH-1015, Lausanne, Switzerland*

[*] - Corresponding author: suvorova@crys.ras.ru. Current address: A.V. Shubnikov Institute of Crystallography of Russian Academy of Sciences, Leninsky pr., 59, Moscow 119333, Russia.

E-mails:

O. Uvarov: uvarov@kapella.gpi.ru

A. Ovcharov: ovcharov.91@gmail.com

I. Karateev: iaKarateev@gmail.com

A. Vasiliev: a.vasiliev56@gmail.com

V. Skuratov: skuratov@jinr.ru

P. Buffat: philippe.buffat@epfl.ch

EFFECTS of Kr and Xe ION IRRADIATION on the STRUCTURE of Y_2O_3 NANOPRECIPITATES in YBCO THIN FILM CONDUCTORS

Abstract.

The response of Y_2O_3 nanoprecipitates in a 1-μm $YBa_2Cu_3O_{7-x}$ layer from a superconducting wire Ag/YBCO/buffer metal oxides/Hastelloy to 107 MeV Kr and 167 MeV Xe ion irradiation was investigated using a combination of transmission electron microscopy, diffraction and X-ray energy dispersive spectrometry. The direct observation of the radiation induced tracks in Y_2O_3 nanocrystals is reported for the first time to the best authors' knowledge. Structureless damaged regions of 5-9 nm (average 8 nm) in diameter were observed in Y_2O_3 nanocrystals when the electronic stopping power S_e was about or higher than 4.7 keV/nm. This value of S_e is the upper estimate of the minimum electronic stopping power to create damage in yttria nanocrystals. The electron diffraction patterns and HRTEM/HRSTEM Fourier transform patterns from areas extending a few nanometers around the tracks show that yttria and YBCO keep their respective cubic and orthorhombic pristine structures.

Keywords: yttria, YBCO, Kr and Xe ions, radiation damage, transmission electron microscopy, electron diffraction.

1. Introduction

Yttria (Y_2O_3) nanoprecipitates play a critical role in a number of composite materials, such as oxide dispersion strengthened alloys where precipitates can dissolve depending on irradiation conditions [1] and $YBa_2Cu_3O_{7-x}$-based high temperature superconductors (YBCO HTS). In YBCO HTS, they attract attention to their possible role as flux pinning centers [2, 3]. Yttria precipitates of nanometer size may form due to deviations from the exact 1:2:3 YBCO

stoichiometry during synthesis, for instance by an excess of yttrium precursor in metalorganic chemical vapor deposition [4].

Heavy-ion irradiation with low fluences [5] is a potential way to improve further the critical current density by creating extra pinning centers with controlled diameters, direction and continuity [6]. In our previous work on the silver coated $YBa_2Cu_3O_{7-x}$ superconducting film deposited on a buffer and Hastelloy, we found that irradiation with 107 MeV $^{84}Kr^{17+}$ (~$2\cdot10^{10}$ and ~$6\cdot10^{10}$ cm^{-2} fluences**)** increased the critical current by 5%, while the transition temperature remained the same as for non-irradiated samples (90 K), and the adhesion at the Hastelloy / buffer interface improved significantly [7]. Transmission electron microscopy (TEM) and X-ray energy dispersive spectrometry (EDS) investigation show that irradiation under such conditions creates spherical or prolate damaged regions of 3-5 nm in diameter in the YBCO grains. In the absence of any diffraction contrast or lattice image contrast they are considered as structureless while the surrounding matter retains the pristine YBCO orthorhombic structure Pmmm [8]. The present work extends the investigation to the irradiation damage in the buried Y_2O_3 nanocrystals.

The cubic form of yttria (space symmetry group Ia) [9] is the most stable structure up to a temperature of 2705 K [10]. Swamy et al [11] reported that above this temperature it was believed that cubic form transforms to the hexagonal structure. A phase transformation from the cubic a to monoclinic phase (space group C2/m) has been induced by dynamic compression (shock-loading to 12-25 GPa) of a sintered powder in a propellant gun [12] or high energy ball milling powders of 50 μm particles [13]. Alternatively, yttria nanocrystals with monoclinic structure can be directly synthesized using furnace-based heating and condensation [14], ultra-fine yttrium particles oxidation [15], flame aerosol [16] and gas phase flame methods [17]. The reverse transition is reported when yttria in monoclinic phase, stable at a 2.5 GPa static pressure

and 1273 K temperature and higher, is annealed in air at 1000°C and atmospheric pressure for several hours [18].

A phase transition from the normal cubic yttria structure to the monoclinic high temperature/high pressure induced by swift ions irradiation at room temperature and pressure is reported for Mo [19, 20], Pb [20, 21], S, Cd, Ta [20, 22], and Xe [23] ions of different energies (electronic stopping powers in the range 3 to 38 keV·nm^{-1}) and fluences (from $0.3 \cdot 10^{12}$ to $1 \cdot 10^{16}$ cm^{-2}). These studies were performed by X-ray diffraction (XRD) and the most prominent changes on diffraction patterns were observed in samples prepared by sintering yttria nanoparticles obtained by ball-milling coarser powders [19, 20, 22] whereas additional observation on thin yttria sputtered coatings on silicon were obtained in [23] by SAED/TEM and EELS. The transformation mechanism under irradiation was attributed to an abrupt increase of the lattice temperature up to melting in a cylindrical region around the ion path followed by a rapid quenching together with an induced pressure wave that could trig the cubic to monoclinic transition in the whole nanocrystal about 20 nm or less in size [21].

However, Som et al. [24–26] did not observe any cubic - monoclinic phase transformation. in Y_2O_3 doped phosphors powders after irradiation by energetic Ni^{7+} (S_e~11.5 keV/nm), Ag^{9+} (S_e~18.2 keV/nm) and Au^{8+} (S_e~20.8 keV/nm) ions with fluences ranged from $1 \cdot 10^{11}$ to $1 \cdot 10^{13}$ ions/cm^2. Instead they report a reduction in particle size from 65 nm to 20 nm (mode diameters in histograms) that they attributed to the fragmentation of grains under the swift heavy ion irradiation.

Beside the aspect of pinning flux in superconductors, a better knowledge on the possible phase transition in yttria nanoprecipitates induced by irradiation is also highly desirable with regard to mechanical properties since this transformation is accompanied by a density increase from 5.032 to 5.468 g/cm^3 and a molecular volume decrease by about 8 % [18, 14].

Several experimental techniques can be used to gather information on the electronic stopping power threshold or the size of the region damaged by irradiation like Rutherford backscattering spectrometry in channeling geometry [27, 28], atomic force microscopy [29, 30], profilometry [31], X-ray diffraction [32], Mössbauer spectroscopy [33], transmission electron microscopy [34, 35]. Their results are most often partial and require indirect interpretation based on models with exception of transmission electron microscopy (TEM) that provides a direct access to morphological and structural information to the micro- to atom scale.

Yttria is one of the materials whose parameters based on direct observation of latent tracks are still missing. The present TEM study is aimed at a characterization of damaged regions in Y_2O_3 nanoprecipitates in YBCO layer after irradiation by ^{84}Kr and ^{131}Xe ions with different energies and finding the electronic energy loss (or electronic stopping power S_e) threshold for track formation. A particular attention was also given toward the stability of yttria nanoprecipitates in order to ascertain the existence or absence of the cubic to monoclinic transition.

2. Materials and methods

The studied 2G HTS tapes from Super Power Inc. are made of a silver cap, a 1μm thick YBCO film, a multilayer buffer metal oxides $LaMnO_3$ / MgO / Y_2O_3 / Al_2O_3) and a 100 μm thick Hastelloy substrate. Coupons of size 1.0 x 0.5 cm^2 were irradiated at room temperature with 167 MeV $^{131}Xe^{27+}$ and 107 MeV $^{84}Kr^{17+}$ ions to fluences of 10^{11} cm^{-2} and 5×10^{11} cm^{-2} in the IC-100 cyclotron at the Flerov Laboratory of Nuclear Reactions of the Joint Institute for Nuclear Research. To prevent sample heating the samples were mounted with double sided carbon tapes on water-cooled copper holders kept at 20 °C and irradiated by scanning Xe and Kr ion over the whole specimen surface with an average ion flux of 2×10^8 $cm^{-2}s^{-1}$. In order to get energies lower than those of the primary 1.2 MeV/amu beams, aluminum degraders 6.5 and 9.5 μm thick were

used to lower the primary ion energy to that chosen for irradiation. The energy lowering by the degraders and the electronic stopping power S_e were calculated using the SRIM2013 code [36].

The dispersion and structure of the yttria nanocrystals in YBCO before and after irradiation was investigated by conventional TEM and scanning TEM (STEM) Bright and High Angle Annular Dark Field modes (BF STEM and HAADF STEM) and Selected Area Electron Diffraction (SAED) under a Tecnai Osiris/FEI microscope (200 kV with a high brightness X-FEG field emission gun). The study of the structure down to the atom level was carried out by High-Resolution Transmission Electron Microscopy (HRTEM), BF and HAADF HRSTEM under a Titan G^3 80 - 300 kV/FEI and a Libra 200 FE HR/Zeiss 200 kV microscope. Care was taken to prevent electron irradiation damage using an illumination intensity as low as possible, avoiding unnecessary exposition to the beam during the search and setup and a short exposure time to record images.

The elements distribution in the layered structure of the tape was observed with an EDS ChemiSTEM X-ray energy dispersive spectrometer fitted on Osiris (0.9 sr collection angle Super-X/FEI with 4 30mm^2 detectors at 22° take-off angle and Esprit 1.9 Quantax/Bruker quantification software).

Thin samples for (S)TEM were prepared in plan-view and cross-sections. Mechanical polishing from the tape substrate side followed by 6 keV Ar ion milling (Gatan) at room temperature (reduced to 1 keV and about 1° grazing incidence for final polishing) was used for plan-view samples. Their wedge-shaped electron transparent area over a few μm along the edge combines the advantages of a large field of view and the choice of the most suitable thickness between 10 and ~70 nm for HRTEM and the defect distribution observation respectively. Alternatively a FEI Helios Nanolab 600i and a FEI Versa 3D DualBeam scanning electron ion

microscopes/focused ion beams were used to get cross-sections and plan-view lamellas with a constant thickness of approximately 30 - 40 nm.

Prior to interpretation, the Gatan Digital Micrograph software (Gatan, Inc., Pleasanton, CA, USA) was used to optimize image contrast, reduce noise and calculate Fast Fourier Transform (FFT) diffractograms from HRTEM and HRSTEM images. Crystal structure determination was obtained from indexing SAED and FFTs patterns with the Java Electron Microscopy Software (JEMS) [37] using the crystal data for cubic and monoclinic Y_2O_3, and orthorhombic YBCO (**Table 1**) from the ICSD database (FIZ Karlsruhe).

3. Results and Discussion

Figure 1a shows a HAADF STEM cross-section overview of the whole layer structure of the tape parallel to the irradiation direction. Yttria nanoprecipitates are visible with a higher magnification in the HAADF STEM image (Fig.1b) and X-ray EDS element map (background counts subtracted) (Fig.1c). They are mainly lying in randomly distributed planes parallel to the layered structure of the tape. This behavior is consistent with the hypothesis that yttria precipitates form because of fluctuations of the yttrium precursor pressure during YBCO deposition. The BF TEM image (Fig.1d) shows parallel columnar tracks left by 167 MeV Xe ions in YBCO and in Y_2O_3 precipitates.

The profiles of energy loss *dE/dx* of ions to the target electrons (or electronic stopping power S_e) along the Kr or Xe ion track were calculated with the SRIM program for a model of 2 μm thick Ag coating on a 1 μm thick YBCO layer containing two 20 nm thick yttria buried 300 and 700 nm below the Ag/YBCO interface (Fig. 2). It shows that the energy of ions slowly decreased with abrupt jumps at the transition between adjacent materials (Ag and YBCO layers, YBCO matrix and Y_2O_3 nanocrystals, YBCO layer and buffer layer). Owing to the small thickness of the yttria layers, ions have nearly the same energy at their entrance and exit faces.

According to the data given by Tombrello [41] we can expect nearly continuous tracks if electronic *dE/dx* is between 30 and 20 keV/nm. Ions with lower initial energies provide isolated damaged regions in the form of ellipsoids (*dE/dx* is between 10 and 20 keV/nm) or spheres (*dE/dx* is below 10 keV/nm). In this work, nearly continuous columnar tracks along the ion's path were observed in the YBCO layer (Fig.1d) irradiated with 167 MeV ($21.9 \leq dE/dx \leq 20.0$ keV/nm after the Ag layer) Xe ions.

Heavy ion-induced damaged regions were observed in tapes irradiated by Kr (107 and 45 MeV) and Xe (167, 77 and 46 MeV) ions with energies corresponding energy deposition of about 4.7 keV/nm or higher. This value of electronic stopping power S_e is the upper estimate of the minimum electronic stopping power to create damage in yttria nanocrystals. Table 2 summarizes ion's energy and ion's energy loss to electrons at which defects in crystals were observed.

Figure 3a is a BF TEM plan-view image of a [001] YBCO layer irradiated with 107 MeV Kr ions. Its characteristic domain structure is seen along or close to [001], 3 - 5 nm rounded irradiation damage regions and yttria nanoprecipitates are present in the imaged area. The white arrows point on healthy precipitates and the white-black one point on a Y_2O_3 precipitate struck by an ion. The 5 - 20 nm Y_2O_3 precipitates are semi-coherent with the matrix and easily observed in domains with diffraction contrast thanks to Moiré fringes. The SAED pattern (Fig.3b) contains strong reflections from [001] YBCO and weak reflections from cubic Y_2O_3 precipitates seen along their <001> and <101> zone axis. Some YBCO and Y_2O_3 reflections are superimposed due to their close interplanar spacings, for instance, (010) and (100) of YBCO with (220) of Y_2O_3 (0.3872, 0.3823 and 0.3749 nm respectively). The detailed indexations are given in Fig. 3c, 3d and 3e leading to 3 orientation variants: $[001](200)Y_2O_3//[001](110)$YBCO and $[101](020)Y_2O_3//[001](010)$YBCO and $[\bar{1}01](101)Y_2O_3$ // $[001](010)$YBCO in agreement with [4].

The diffraction conditions of imaging the sample oriented along the exact zone axis or close to it are well suited for obtaining two-phase SAED patterns for unambiguous identification of YBCO and Y_2O_3 phases and their crystallographic orientation relationships. The irradiation-induced damaged regions are visible as 3 - 5 nm bright spots in diffracting YBCO grains (dark area) and are not or hardly visible elsewhere where the orientation is far from strong diffraction conditions that leads only to weak mass scattering contrast (Fig. 3 a).

Figure 4 shows plan-views of the YBCO matrix with healthy yttria nanocrystals indicated with white arrows, damaged yttria nanocrystals (white-black arrows) and damaged regions (bright or black rounded contrasts in BF TEM or HAADF STEM images respectively) induced by Xe ions with energies of 167 MeV (Fig. 4a), 77 MeV (Fig.4b) and 46 MeV (Fig.4c). Yttria nanocrystals have parallelepiped shapes and sizes of about 5÷10 nm x 5÷10 nm x 10÷20 nm in the whole sample

To estimate the density of damaged regions, yttria nanocrystals and relative part of yttria nanocrystals struck by swift heavy ions in YBCO, high resolution TEM and STEM images were obtained with magnification suitable to distinguish radiation damaged regions from yttria nanocrystals of the similar size. The density of precipitates and damaged regions was measured by averaging over several images for each ion energy. It was found that precipitates have the density of about $0.5 – 1.8 \cdot 10^{11}$ cm^{-2} in projection of the 30-40 nm thick sample. This is rather rough estimate because of the nonhomogeneous distribution of yttria nanocrystals in the YBCO volume. The density of radiation defects is found to be $0.9 – 1.4 \cdot 10^{11}$ cm^{-2} in projection for all samples what corresponds to fluences applied in this work within the measurement uncertainties. Comparative analysis showed that sizes, distributions and shapes of yttria nanoprecipitates before and after irradiation remained essentially unchanged as well no evidences were obtained for

irradiation induced precipitation. These results are consistent with the observations of Little et al. [42] in the study of irradiation effects on microstructure of yttria containing ODS alloys.

Analysis of (S)TEM images showed that about 12 – 25 % of yttria precipitates were struck by ions. However, the occurrence of an ion interaction in the yttria nanoprecipitate center is seldom owing to the close size between the irradiation region diameter and the yttria precipitate width. Therefore, most events extend in both YBCO and yttria across their interface. Figures 5a and 5c show two high resolution BF STEM images where damaged regions induced by 167 MeV Xe ions are lying in the Y_2O_3 precipitate (Fig. 5a) or at the YBCO – Y_2O_3 interface (Fig. 5c). Fig. 5b and 5b' are FFT of the whole area of Fig. 5a for the two orientation variants [001](020)Y_2O_3 // [001](110)YBCO and <101>(020)Y_2O_3 // [001](010)YBCO. The two yttria precipitates d and e in Figure 5c were damaged by ions travelling close to their corners. It is worth noting that these corners are crystalline and spill out onto circular projection of the damaged region in YBCO. The BF HRSTEM image and FFT's from the corresponding square areas (Fig. 5d and 5e) confirm that precipitates retained their pristine cubic structure after damage. Another damaged region on top of figure 5a lies along an yttria/YBCO interface. Together with precipitates d and e it shows that the damage does not extend deep in yttria when the ion trajectory is close but outside the precipitate. That can be understood as a higher resistance of yttria than that of YBCO to damage by a radiation excitation stemming from YBCO.

Figures 6a shows the HRSTEM image of the damaged area when a 167 MeV Xe ion passed through an yttria precipitate. The FFT pattern in Figure 6b was obtained from a reduced area (4 x 4) nm^2 at the arrow tip pointing to the undamaged part of the Y_2O_3 nanoprecipitate while the FFT pattern of Figure 6c was taken from the square area around the whole Y_2O_3 nanocrystal, its damaged region and the surrounding YBCO matrix. From the center of mass of the damaged region the ion trajectory was inside the precipitate at a distance about 1nm or

slightly larger from its interface with YBCO. The lattice image contrast disappeared in both phases to let a structureless circular area of about 7.5 - 8 nm diameter (Fig.6 d) in contrast with the damage areas of the top precipitate in fig 5a and precipitates d and e in fig. 5c. The absence of a visible YBCO lattice structure in this region implies that its volume extends through most if not all the TEM sample thickness and that therefore it has a prolate ellipsoid or tube shape with its axis parallel to the ion trajectory.

HRTEM observation (Fig. 7a) is confirming the extension of the damaged volume in both phases when an ion is passing through the center of a precipitate. The FFT pattern of Fig. 7b was taken from the square areas around the whole Y_2O_3 nanocrystal, its damaged region and the surrounding YBCO matrix. All FFTs (Fig. 6b and 6c; Fig. 7b) show that Y_2O_3 nanocrystals keep their cubic structure in orthorhombic YBCO with the epitaxial orientation relations <101>(020) Y_2O_3//[001](010) YBCO.

Thus TEM, HRSTEM and electron diffraction show that both Y_2O_3 nanocrystals and YBCO matrix retain their pristine structure out of the tracks (cubic [14] and orthorhombic [8], respectively) under all irradiation conditions applied in this work. The presence of tracks was observed in Y_2O_3 nanoparticles with an electronic stopping power as small as S_e = 4.7 keV/nm, which may be considered as an upper estimate of the minimum energy loss for track formation. In this work, the electron diffraction patterns and HRTEM/HRSTEM FFTs did not show the phase transformation from cubic to monoclinic structure in Y_2O_3 nanoprecipitates. We suggest that the cubic to monoclinic phase transformation observed by XRD in yttria under irradiation reported in the literature [19-22] may result of a synergy effect between irradiation and the presence in the original material of monoclinic seeds, crystal defects or stresses after the mechanical preparation [43].

More experimental investigation are planned to get the precise chemical composition of the amorphous track content and structure of the track wall.

4. Conclusions

High energetic heavy Kr and Xe ions induce the formation of damaged regions in yttria nanoprecipitates buried in YBCO layer when the specific ionization energy loss is about or above 4.7 keV/nm. No radiation damage in YBCO and Y_2O_3 precipitates was observed with 23 MeV Kr ions ($3.7 \leq dE/dx \leq 1.8$ keV/nm). The damaged regions are tubes or prolate ellipsoids in the direction of the ion trajectory. Lattice image contrast and diffraction contrast have disappeared in such regions to let structureless circular areas about 6-9 nm in diameter that confirms they contain an amorphous material and extend through the whole thickness of the yttria precipitates and beyond into YBCO. When ions travel in YBCO very close to an interface with yttria or corner the damaged regions extend only very little in yttria. This could be understood as if the perturbation stemming from YBCO does not propagate easily in yttria, or as yttria is more resistant to it. The electron diffraction and HRTEM/HRSTEM Fourier transform patterns from areas extending a few nanometers around the track shows that yttria and YBCO have the same yttria cubic and YBCO orthorhombic structures as before irradiation. The Y_2O_3 – YBCO crystallographic orientation relationships remained unchanged.

Acknowledgements

The authors greatly appreciate the discussion of the results with Professor A.E. Volkov (Lebedev Physical Institute of the Russian Academy of Sciences, Russia). We thank Dr. N.B. Bolotina for English editing this manuscript.

References

1. I. Monnet, P. Dubuisson, Y. Serruys, M. O. Ruault, O. Kaïtasov, and B. Jouffrey, *Microstructural investigation of the stability under irradiation of oxide dispersion strengthened ferritic steels*, J. Nucl.Mat. 335 (2004), pp. 311-321

2. K. Verbist, A. L. Vasiliev, and G. Tendeloo, *Y_2O_3 inclusions in $YBa_2Cu_3O_{7-\delta}$ thin films*, Appl. Phys. Lett. 66 **(**1995), pp. 1424-1427

3. Y. Q. Li, J. Zhao, C. S. Chern, P. Lu, T. R. Chien, B. Gallois, P. Norris, B. Kear, and F. Cosandey, *Effects of Y_2O_3 precipitates on critical current anisotropy in $YBa_2Cu_3O_{7-x}$ thin films prepared by plasma enhanced metalorganic vapor deposition*, Appl. Phys. Lett. 60 (1992), pp. 2430-2432

4. P. Lu, Y. Q. Li, J. Zhao, C. S. Chern, B. Gallois, P. Norris, B. Kear, and F. Cosandey, *High density, ultrafine precipitates in $YBa_2Cu_3O_{7-x}$ thin films preparedby plasma-enhanced metalorganic chemical vapor deposition*, Appl. Phys. Lett. 60 (1992), pp. 1265-1267

5. B. Roas, B. Hensel, S. Henke, S. Klaumünzer, B. Kabius, W. Watanabe, G. Saemann-Ischenko, L. Schultz, and K. Urban, *Effects of 173 MeV 129Xe ion irradiation on epitaxial YBa2Cu3Ox films*, Eurphys. Lett. 11 (1990), pp. 669-674

6. R. Weinstein, D. Parks, R-P. Sawh, B. Mayes, A. Gandini, A. Goyal, Y. Chen, and V. Selvamanickam, *Effects on J_c of pinning center morphology for multiple-in-line-damage in coated conductor and bulk, melt-textured HTS*, Physica C 469 (2009), pp. 2068-2076

7. E. I. Suvorova, M. Cantoni, P. A. Buffat, A.Y. Didyk, L. K. Antonova, A.V. Troitskii, and G. N. Mikhailova, *Structure analysis of the YBCO layer in Ag/YBCO/metal oxide buffer/Hastelloy composite tape before and after 107 MeV Kr^{17+} irradiation*, Acta Mat. 75 (2014), pp. 71-79

8. D. C. Johnston, A. J. Jacobson, J. M. Newsam, J. T. Lewandowski, D. P. Goshorn, D. Xie, and W. B. Yelon, *Variation in the Structural, Magnetic, and Superconducting Properties of*

$YBa_2Cu_3O_{7-x}$ with Oxygen Content. Chapter 14. ACS Symposium Series, 351 (1987), pp. 136-151

9. M. G. Paton, and E.N. Maslen, *A refinement of the crystal structure of yttria*, Acta Cryst. 19 (1965), pp. 307-310

10. V. Swamy, N. A. Dubrovinskaya, and L. S. Dubrovinsky, *High-temperature powder X-ray diffraction of yttria to melting point*, Mater. Res. 14 (1999), pp. 456-459

11. V. Swamy, H. J. Seifert, F. Aldinger, *Thermodynamic properties of Y_2O_3 phases and the yttrium–oxygen phase diagram*, J. Alloys Comp. 269 (1998), pp. 201–207

12. T. Atou, K. Kusaba, K. Fukuoka, M. Kikuchi, and Y. Syono, *Shock-induced phase transition of M203 (M = Sc, Y, Sm, Gd, and In) - type compounds*, J. Solid State Chem. 89 (1990), pp. 378-384

13. M. K. Lee, E. K. Park, J. J. Park, and C. K. Rhee, *Control of Y_2O_3 phase and its nanostructure formation through a very high energy mechanical milling*, J. Solid State Chem. 201 (2013), pp. 56-62

14. W. Krauss, and R. Birringer, *Metastable phases synthesized by inert-gas-condensation*, Nanostruct. Mater., 9 (1–8) (1997), pp. 109-112

15. G. Skandan, C. M. Foster, H. Frase, M. N. Ali, J. C. Parker, and H. Hahn, *Phase characterization and stabilization due to grain size effects of nanostructured Y_2O_3,* Nanostruct. Mater. 1 (1992), pp. 313- 322

16. B. Guo, M. Mukundan, and H. Yim, *Flame aerosol synthesis of phase-pure monoclinic Y_2O_3 particles via particle size control*, Powder Technology 191 (2009), pp. 231-234

17. P. Zhang, A. Navrotsky, B. Guo, I. Kennedy, A. N. Clark, C. Lesher, and Q. Liu, *Energetics of Cubic and Monoclinic Yttrium Oxide Polymorphs: Phase Transitions, Surface Enthalpies, and Stability at the Nanoscale*, J. Phys. Chem. C 112 (2008), pp. 932-938

18. H. R. Hoekstra, and K. A. Gingerich, *High-Pressure B-type polymorphs of some rare-earth sesquioxides*, Science, 146 (1964), pp. 1163-1164

19. S. Hémon, Ch. Dufour, A. Berthelot, F. Gourbilleau, E. Paumier, and S. Bégin-Colin, *Structural transformation in two yttrium oxide powders irradiated with swift molybdenum ions*, Nucl. Instr. Meth. Sect. B, 166-167 (2000), pp. 339-344

20. S. Hémon, A. Berthelot, Ch. Dufour, F. Gourbilleau, E. Dooryhée, S. Bégin-Colin, and E. Paumier, *Influence of the crystallite size on the phase transformation of yttria irradiated with swift heavy ions*, Eur. Phys. J. B **19** (2001), pp. 517-523

21. S. Hémon, Ch. Dufour, F. Gourbilleau, E. Paumier, E. Dooryhée, and S. Bégin-Colin, *Influence of the grain size: yttrium oxide irradiated with swift heavy ions*, Nucl. Instr. Meth. Sect. B, 146 (1998), pp. 443-448

22. S. Hémon, V, Chailley, E. Dooryhée, Ch. Dufour, F. Gourbilleau, F. Levesque, and E. Paumier, *Phase transformation of polycrystalline Y_2O_3 under irradiation with swift heavy ions*, Nucl. Instr. Meth. Sect. B 122 (1997), pp. 563-565

23. R.J. Gaboriaud, M. Jublot, F. Paumier, and B. Lacroix, *Phase transformations in Y_2O_3 thin films under swift Xe ions irradiation*, Nucl. Instr. Meth. Phys. Res. Sect. B 310 (2013), pp.6-9

24. S. Som, S. K. Sharma, S. P. Lochab, *Ion induced modification of band gap and CIE parameters in $Y_2O_3:Dy^{3+}$ phosphor*, Ceramics International 39 (2013), pp. 7693-7701

25. S. Som, S. K. Sharma, and S. P. Lochab, *Swift heavy ion induced structural and optical properties of $Y_2O_3:Eu^{3+}$ nanophosphor*, Materials Research Bulletin 48 (2013), pp. 844-851

26. S. Som, S. Das, S. Dutta, M. K. Pandey, R. K. Dubey, H. G. Visser, S. K. Sharma, and S. P. Lochab, *A comparative study on the influence of 150 MeV Ni^{7+}, 120 MeV Ag^{9+}, and 110 MeV Au^{8+} swift heavy ions on the structural and thermoluminescence properties of Y_2O_3: Eu^{3+}/Tb^{3+} nanophosphor for dosimetric applications*, J Mater Sci 51 (2016), pp. 1278-1291

27. N. Mejai, A. Debelle, L. Thomé, G. Sattonnay, D. Gosset, A. Boulle, R. Dargis, and A. Clark, *Depth-dependent phase change in Gd_2O_3 epitaxial layers under ion irradiation*, Appl. Phys. Let. 107 (2015), no. 131903

28. T. Steinbach, Th. Bierschenk, S. Milz, M. C. Ridgway, and W. Wesch, *Swift heavy ion irradiation of crystalline CdTe*, J. Phys. D: Appl. Phys. 47 (2015), no. 065301

29. N. Khalfaoui, J. P. Stoquert, F. Haas, C. Traumann, A. Meftah, and M. Toulemonde, *Damage creation threshold of Al_2O_3 under swift heavy ion irradiation*, Nucl. Instr. and Meth. B 286 (2012), pp. 247-253

30. A. H. Mir, I. Monnet, M. Toulemonde, S. Bouffard, C. Jegou, and S. Peuget, *Mono and sequential ion irradiation induced damage formation and damage recovery in oxide glasses: Stopping power dependence of the mechanical properties*, J. Nucl. Mater. 469 (2016), pp. 244-250

31. J-M. Costantini, C. Trautmann, L. Thome, J. Jagielski, and F. Beuneu, *Swift heavy ion-induced swelling and damage in yttria-stabilized zirconia*, J. Appl. Phys. 101**(**2007), no. 073501

32. K. Nakano, H. Yoshizaki, Y. Saitoh, N. Ishikawa, and A. Iwase, *XRD study of yttria stabilized zirconia irradiated with 7.3 MeV Fe, 10 MeV I, 16 MeV Au, 200 MeV Xe and 2.2 GeV Au ions*, Nucl. Instrum. Methods Phys. Res., Sect. B 370 (2016), pp. 67-72

33. S. Stichleutner, E. Kuzmann, K. Havancsák, Z. Homonnay, A. Vértes, O. Doyle, M. El-Sharif, and C. U. Chisholm, *Mössbauer studies of the effect of swift heavy ion irradiation on electrodeposited Sn-Co-Fe coatings*, J. Phys. Conf. Ser., 217 **(**2010), no. 012100

34. T. Aruga, Y. Katano, T. Ohmichi, S. Okayasu, and Y. Kazumata, *Amorphization behaviors in polycrystalline alumina irradiated with energetic iodine ions*, Nucl. Instrum. Methods Phys. Res., Sect. B 166-167 (2000), pp. 913-919

35. V. A. Skuratov, A. S. Sohatsky, J. H. O'Connell, K. Kornieieva, A. A. Nikitina, J. H. Neethling, and V. S. Ageev, *Swift heavy ion tracks in $Y_2Ti_2O_7$ nanoparticles in EP450 ODS steel*, J. Nucl. Mater., 456 (2015), pp. 111-114

36. J. F. Ziegler and J. P. Biersack, 2013, *SRIM (The stopping and range of ions in matter*) software available at http://www.srim.org/SRIM/SRIMLEGL.htm

37. P. Stadelmann 2017 JEMS, *Java (Electron Microscopy Software)*; software available at http://www.jems-saas.ch

38. T. Atou, K. Kusaba, K. Fukuoka, M. Kikuchi, K. Fukuoka, and Y. Syono, *Shock-induced phase transition of M2O3 (M = Sc, Y, Sm, Gd, and In)-type compounds*, J. Solid State Chem., 89 (1990), pp. 378 -384

39. V. Srikanth, A. Sato, J. Yoshimoto, J. H. Kim, and T. Ikegami, *Synthesis and crystal structure study of Y_2O_3 high-pressure polymorph*, Cryst. Res. Technol., 29 (1994), pp. 981-984

40. J. Zhang, H. Cui, P. Zhu, C. Ma, X. Wu, H. Zhu, Y. Ma, and Q. Cui, *Photoluminescence studies of Y_2O_3: Eu(3+) under high pressure*, J. Appl.Phys., 115 (2014) no. 023502

41. T. A. Tombrello, *Columnar track damage in YBCO*, Nucl. Instr. Meth. Sect. B, 95 (1995), pp. 232-234

42. E. A. Little, D. J. Mazey, W. Hanks, *Effects of ion irradiation on the microstructure of an oxide-dispersion-strengthened ferritic steel*, Scr. Metall. Mater. 25 (1991), pp. 1115-1118

43. A. Guinier, *X-Ray diffraction in crystals, imperfect crystals, and amorphous bodies*, Dover Publications, New York, 1994

Table 1. Space group and lattice parameters of Y_2O_3 and YBCO

Compound	Space group	Lattice parameters a [nm]	b [nm]	c [nm]	β [°]	Ref.
Y_2O_3	$Ia\bar{3}$	1.060	1.060	1.060	90.0	[9] ICSD 23811
Y_2O_3	C2/m	1.3880	0.3513	0.8629	100.09	[38] ICSD 647650
Y_2O_3	C2/m	1.38714	0.34487	0.85862	100.12	[39]
Y_2O_3	C2/m	1.4060	0. 3536	0.8567	100.0	[40] ICSD 192863
YBCO	Pmmm	0.3824	0.3888	1.1690	90.0	[8] ICSD 63688

Table 2. Energy of Kr and Xe ions and ion's energy loss to electrons *Se* for which radiation induced damaged areas have been observed by (S)TEM.

Ion	Energy of ions entering Ag coating [MeV]	Energy of ions entering YBCO [MeV]	Energy of ions exiting YBCO [MeV]	*Se* (entrance YBCO) [keV/nm]	*Se* (exit YBCO) [keV/nm]	Damaged areas
Xe	167	101	80.6	29.8	16.1	yes
	77	34.4	23.3	15.3	7.5	yes
	46	17.4	11.0	8.9	4.7	yes
Kr	107	62.1	46.7	20.8	14.0	yes
	45	16.4	9.2	7.7	4.6	yes
	23	6.2	3.0	3.9	1.8	no

Figure captions

Figure1. HAADF STEM image of cross-section of the Ag/YBCO/buffer metal oxides/Hastelloy tape. The arrow points to the irradiation direction with 167 MeV Xe ions (a), HAADF STEM image with ~5x5x20nm^3 yttria precipitates (b) and element X-ray EDS map (c), BF/TEM of YBCO with Y_2O_3 and nearly continuous columnar tracks (d).

Figure 2. Calculated profiles of ion's energy loss to electrons across the model multilayer 2 μm Ag / 300 nm YBCO / 20 nm Y_2O_3 / 360 nm YBCO / 20 nm Y_2O_3 / 300 nm YBCO / buffer for 107, 45 and 23 MeV Kr and 167, 77 and 46 MeV Xe ions.

Figure 3. Plan-view BF/TEM image of an irradiated YBCO layer (107 MeV Kr) containing yttria nanoprecipitates revealed by Moiré patterns. The white arrows point on healthy precipitates and the white-black one point on a Y_2O_3 precipitate struck by an ion (a), SAED pattern from the full area of the image (YBCO matrix and Y_2O_3 precipitates) (b), indexing the SAED pattern for 3 different orientation relationships: $[001]Y_2O_3$ // [001]YBCO (c), $[101]Y_2O_3$ // [001]YBCO (d), $[\bar{1}01]Y_2O_3$ // [001] YBCO (e).

Figure 4. Plan view of YBCO matrix with yttria nanocrystals and damaged regions (white and black-white arrows points on healthy and damaged yttria precipitates respectively): the regions damaged by Xe 167 MeV have a dark HAADF STEM contrast (a); the regions damaged by Xe 77 MeV have a bright BF TEM contrast (b); the absence of HAADF HRSTEM atom lattice in the regions damaged by Xe 46 MeV shows that the track extends through the whole TEM sample thickness (c).

Figure 5. BF HRSTEM plan view of yttria in YBCO with irradiation-induced damaged regions by 167 MeV Xe ions close to the precipitate/matrix interfaces (a), corresponding FFT from the full area of (a) showing two orientation variants of yttria $[001]Y_2O_3$//[001]YBCO and $[101]Y_2O_3$//[001]YBCO// (b, b'); BF/HRSTEM image of Y_2O_3 nanocrystals in YBCO with

radiation defects close to corners of the Y_2O_3 (c), corresponding FFTs (d, e) from undamaged parts of yttria nanocrystals in (square areas d and e).

Figure 6. HAADF HRSTEM image of an 8 nm region damaged by a 167 MeV Xe ion passing through an yttria precipitate about 1 nm of its interface with YBCO (a); FFT from the undamaged part of the Y_2O_3 crystal 4 nm x 4 nm at the position of the black-white arrow tip (b); FFT from the square area (c), enlarged and filtered HAADF HRSTEM image highlighting the amorphous structure in the damaged areas (d).

Figure 7. BF HRTEM image of the damage by a 167 MeV Xe ion passing through near to the center of an Y_2O_3 precipitate (a); FFT from the area inside the white square (b); enlarged HRTEM image of amorphous structure in the damaged area in the yttria nanoprecipitate (c).

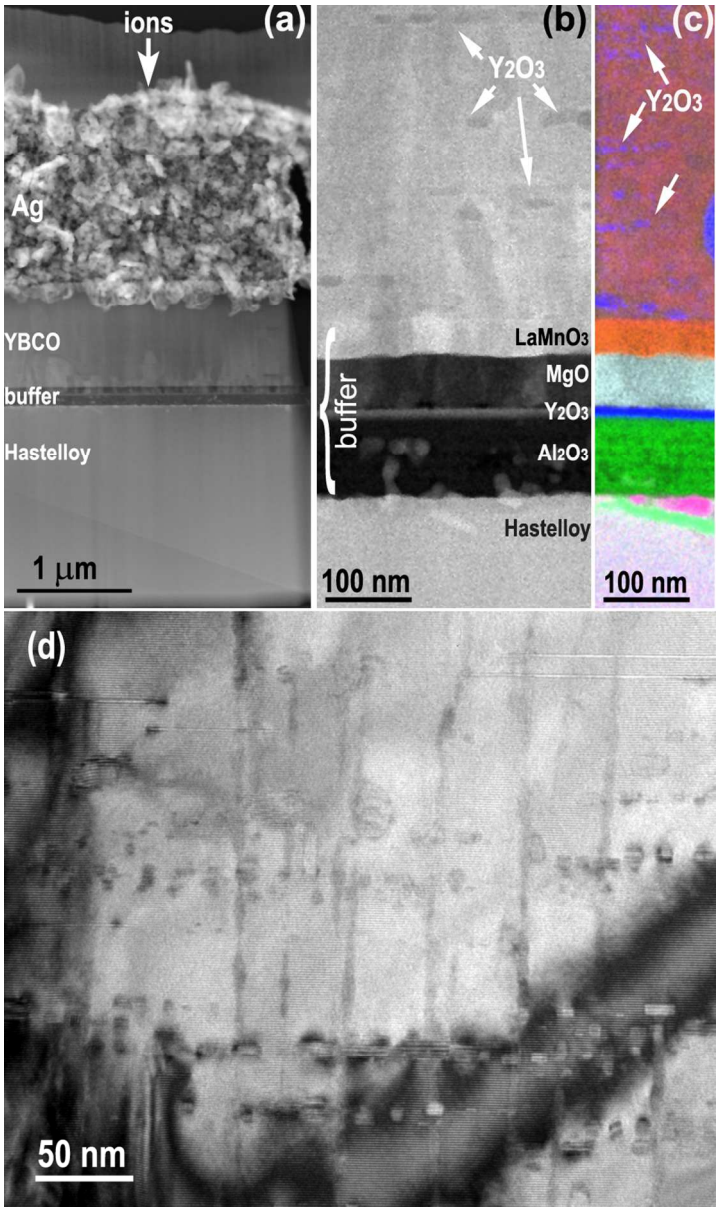

Figure 1.HAADF STEM image of cross-section of the Ag/YBCO/buffer metal oxides/Hastelloy tape. The arrow points to the irradiation direction with 167 MeV Xe ions (a), HAADF STEM image with ~5x5x20 nm3 yttria precipitates (b) and element X-ray EDS map (c), BF/TEM of YBCO with Y2O3 and nearly continuous columnar tracks (d).

120x203mm (202 x 202 DPI)

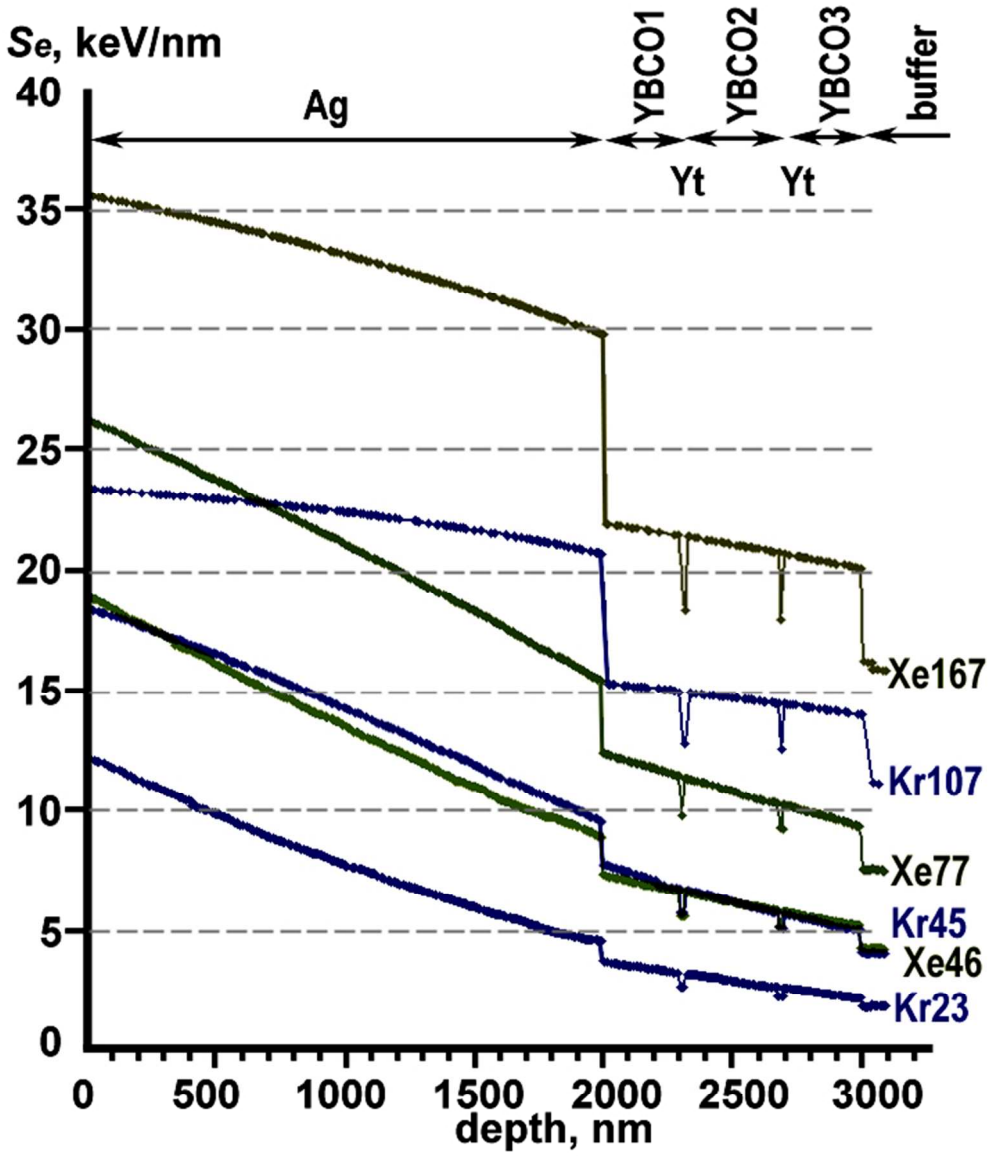

Figure 2. Calculated profiles of ion's energy loss to electrons across the model multilayer 2 μm Ag / 300 nm YBCO / 20 nm Y2O3 / 360 nm YBCO / 20 nm Y2O3 / 300 nm YBCO / buffer for 107, 45 and 23 MeV Kr and 167, 77 and 46 MeV Xe ions.

140x167mm (131 x 131 DPI)

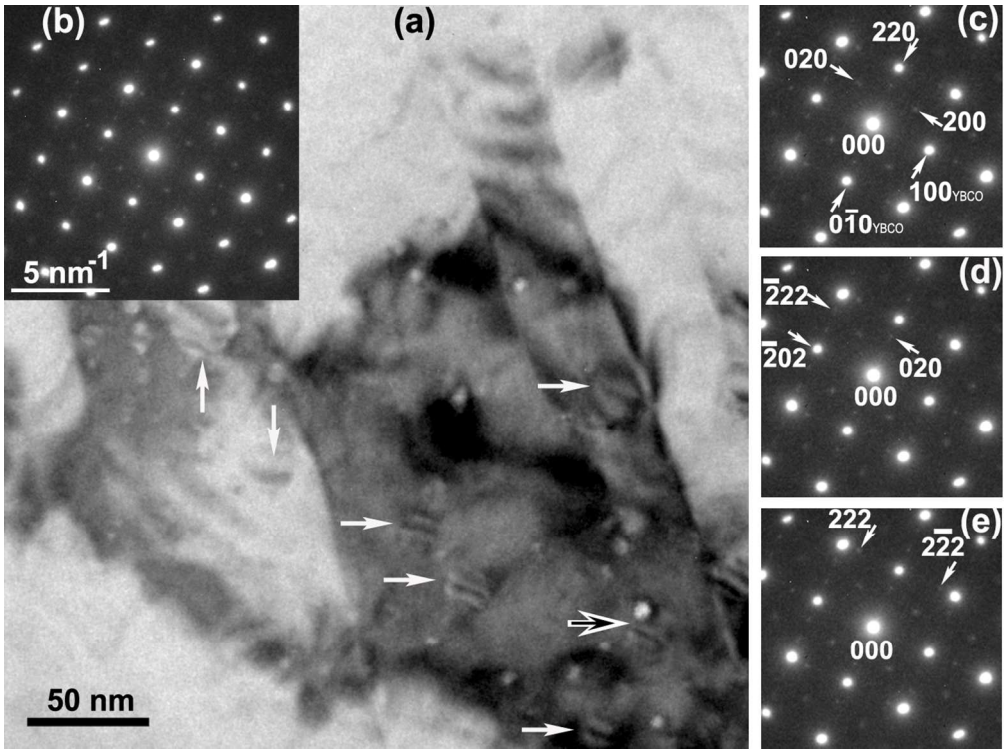

Figure 3. Plan-view BF/TEM image of an irradiated YBCO layer (107 MeV Kr) containing yttria nanoprecipitates revealed by Moiré patterns. The white arrows point on healthy precipitates and the white-black one point on a Y2O3 precipitate struck by an ion (a), SAED pattern from the full area of the image (YBCO matrix and Y2O3 precipitates) (b), indexing the SAED pattern for 3 different orientation relationships: [001]Y2O3 // [001]YBCO (c), [101]Y2O3 // [001]YBCO (d), [-101]Y2O3 // [001] YBCO (e)

120x89mm (290 x 290 DPI)

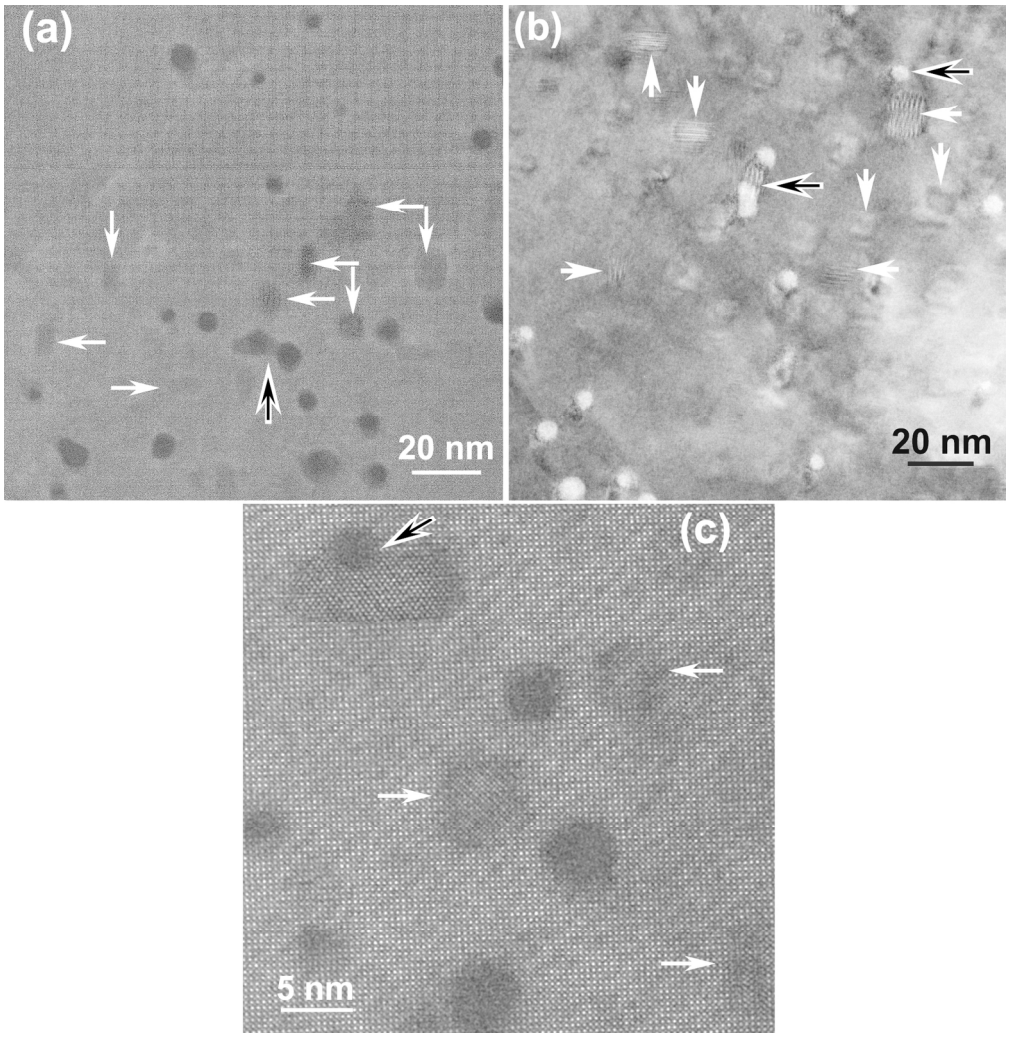

Figure 4. Plan view of YBCO matrix with yttria nanocrystals and damaged regions (white and black-white arrows points on healthy and damaged yttria precipitates respectively): the regions damaged by Xe 167 MeV have a dark HAADF STEM contrast (a); the regions damaged by Xe 77 MeV have a bright BF TEM contrast (b); the absence of HAADF HRSTEM atom lattice in the regions damaged by Xe 46 MeV shows that the track extends through the whole TEM sample thickness (c).

159x163mm (300 x 300 DPI)

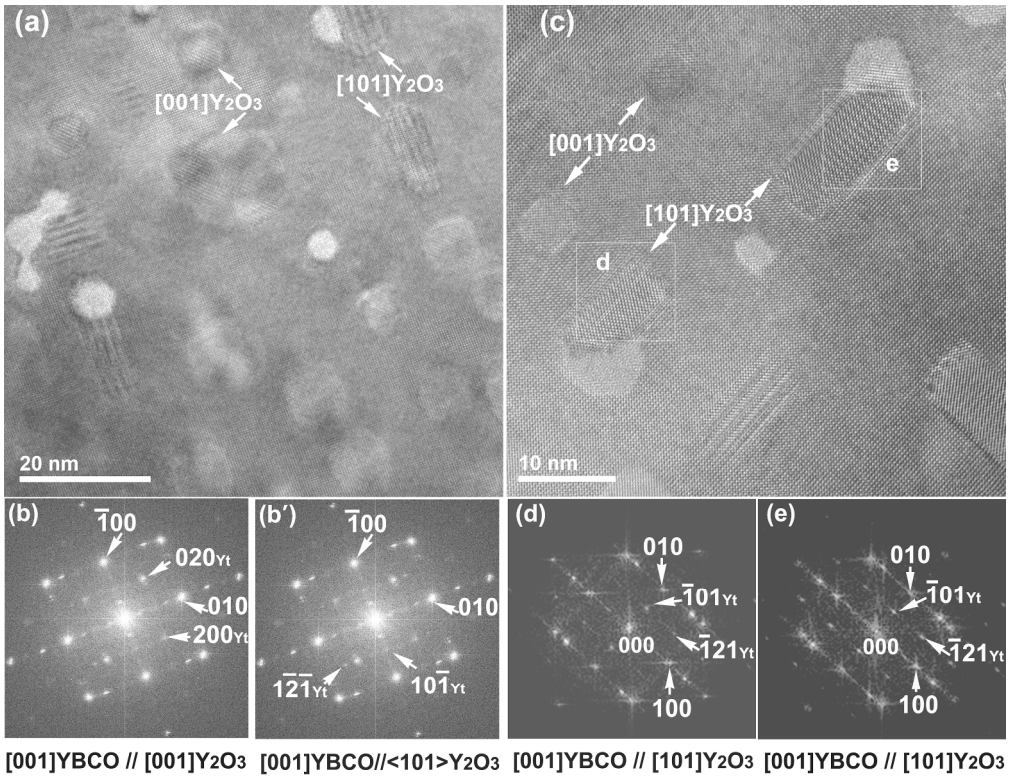

Figure 5. BF HRSTEM plan view of yttria in YBCO with irradiation-induced damaged regions by 167 MeV Xe ions close to the precipitate/matrix interfaces (a), corresponding FFT from the full area of (a) showing two orientation variants of yttria [001]Y2O3//[001]YBCO and [101]Y2O3//[001]YBCO// (b, b'); BF/HRSTEM image of Y2O3 nanocrystals in YBCO with radiation defects close to corners of the Y2O3 (c), corresponding FFTs (d, e) from undamaged parts of yttria nanocrystals in (square areas d and e).

124x96mm (600 x 600 DPI)

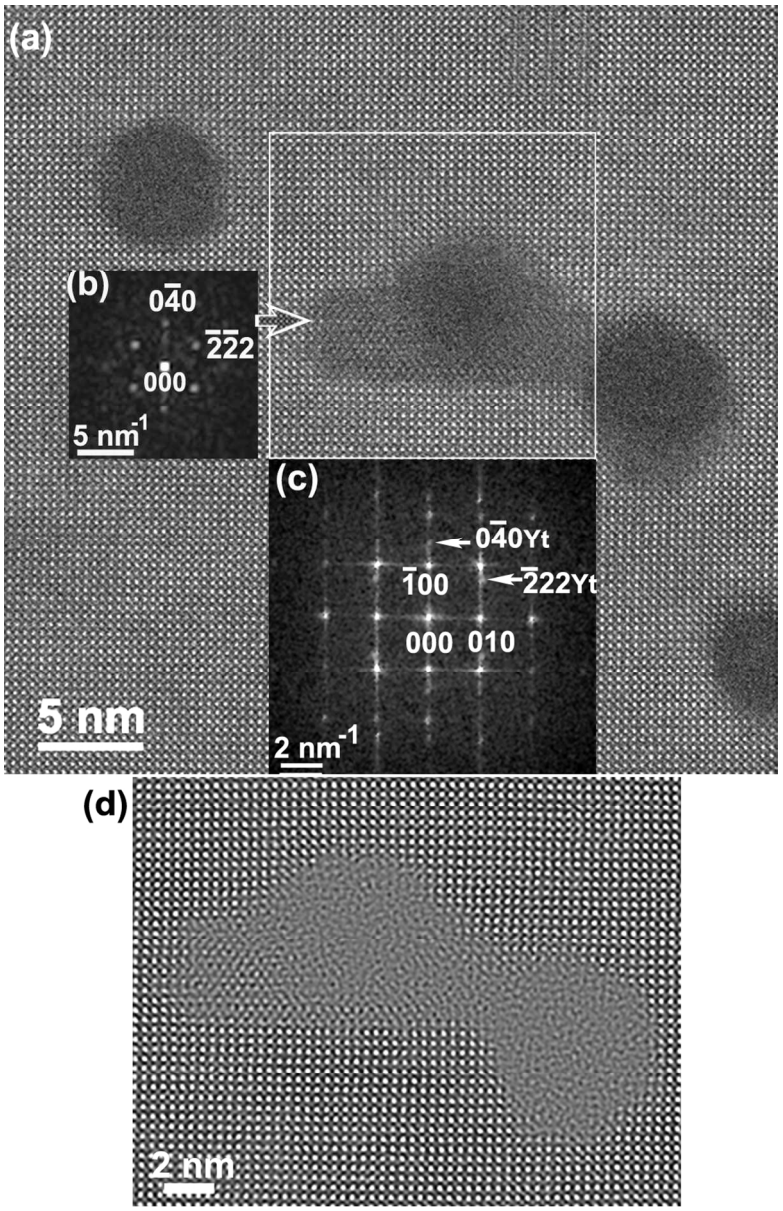

Figure 6. HAADF HRSTEM image of an 8 nm region damaged by a 167 MeV Xe ion passing through an yttria precipitate about 1 nm of its interface with YBCO (a); FFT from the undamaged part of the Y2O3 crystal 4 nm x 4 nm at the position of the black-white arrow tip (b); FFT from the square area (c), enlarged and filtered HAADF HRSTEM image highlighting the amorphous structure in the damaged areas (d).

150x233mm (180 x 180 DPI)

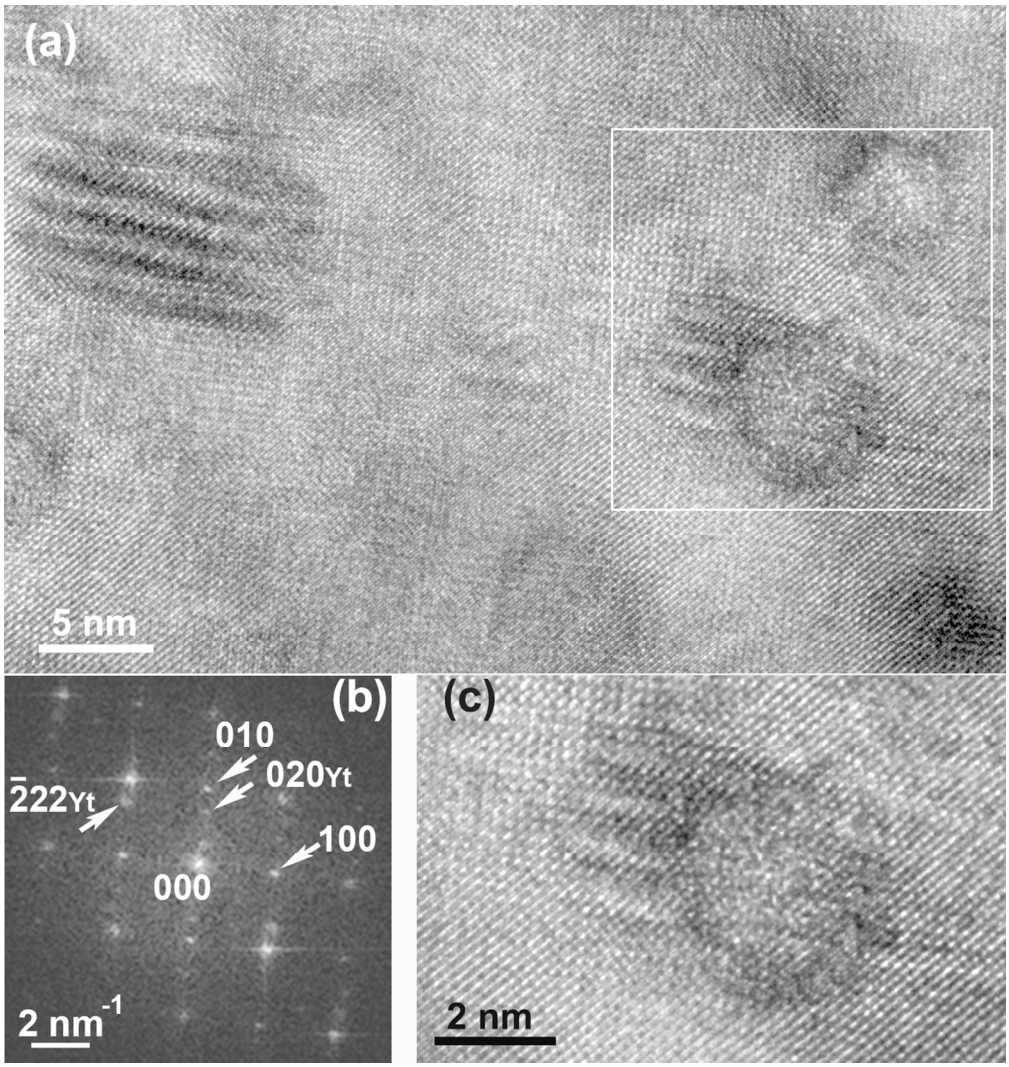

Figure 7. BF HRTEM image of the damage by a 167 MeV Xe ion passing through near to the center of an Y2O3 precipitate (a); FFT from the area inside the white square (b); enlarged HRTEM image of amorphous structure in the damaged area in the yttria nanoprecipitate (c).

160x169mm (214 x 214 DPI)